# Changing Chirality during Single-Walled Carbon Nanotube Growth: A Reactive Molecular Dynamics/Monte Carlo Study

Erik C. Neyts,*,[†] Adri C. T. van Duin,[‡] and Annemie Bogaerts[†]

[†]Research Group PLASMANT, Department of Chemistry, University of Antwerp, Universiteitsplein 1, 2610 Antwerp, Belgium

[‡]Department of Mechanical and Nuclear Engineering, The Pennsylvania State University, University Park, Pennsylvania 16801, United States

ABSTRACT: The growth mechanism and chirality formation of a single-walled carbon nanotube (SWNT) on a surface-bound nickel nanocluster are investigated by hybrid reactive molecular dynamics/force-biased Monte Carlo simulations. The validity of the interatomic potential used, the so-called ReaxFF potential, for simulating catalytic SWNT growth is demonstrated. The SWNT growth process was found to be in agreement with previous studies and observed to proceed

through a number of distinct steps, viz., the dissolution of carbon in the metallic particle, the surface segregation of carbon with the formation of aggregated carbon clusters on the surface, the formation of graphitic islands that grow into SWNT caps, and finally continued growth of the SWNT. Moreover, it is clearly illustrated in the present study that during the growth process, the carbon network is continuously restructured by a metal-mediated process, thereby healing many topological defects. It is also found that a cap can nucleate and disappear again, which was not observed in previous simulations. Encapsulation of the nanoparticle is observed to be prevented by the carbon network migrating as a whole over the cluster surface. Finally, for the first time, the chirality of the growing SWNT cap is observed to change from (11,0) over (9,3) to (7,7). It is demonstrated that this change in chirality is due to the metal-mediated restructuring process.
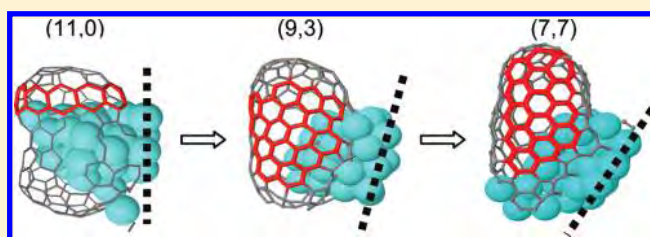
1. INTRODUCTION

Carbon nanotubes (CNTs) continue to attract widespread attention due to their unique properties, which offer perspective on a plethora of applications.[1−3] Examples include their use as interconnects in silicon IC fabrication because of their high current carrying capacity ($>10^9$ A cm^{-2}) or as heat sinks to dissipate heat from computer chips due to their very high thermal conductivity (>3500 W m^{-1} K^{-1}). Especially single-walled carbon nanotubes (SWNTs) offer perspective, since they can be either metallic or semiconducting, depending on their chirality. Furthermore, their chirality distribution and their band gap can be tuned.[4−6] They are envisaged for use in nanoscale electronics such as single-electron transistors, as electron field emitters, for hydrogen storage, as actuators and chemical sensors, in superstrong polymeric composite materials, etc. Currently, however, the applicability of CNTs is limited by a lack of control over their fundamental properties such as the diameter, length, and chirality. Especially for electronic applications, control over these properties is of crucial importance.

A large number of atomistic growth simulations have been carried out in the past in order to obtain insight into the precise growth mechanisms, which is a prerequisite to reach this goal. Gavillet et al. used density functional theory (DFT) simulations to investigate the initial ring formation by cooling a mixed Co/C cluster from 2000 to 1500 K, as well as the elongation of a preformed cap structure by incorporation of carbon atoms at the metal/cap interface.[7,8]

Balbuena et al. and Wang et al. performed DFT calculations on adding C or C_2 units to preformed caps, focusing on the possibility of chirality change. Specifically, Balbuena et al. showed that armchair and near-armchair caps facilitate both thermodynamically and kinetically the addition of C_2 units to their rim sites, offering many more alternative reaction paths than zigzag sites do.[9] Wang et al. showed that chiral selectivity might be obtained by adding C and C_2 units at different ratios during different reaction stages.[10]

A large number of DFT-based tight-binding molecular dynamics (MD) simulations were performed by Page et al. and Ohta et al. on Fe and Ni nanoparticles.[11−15] These simulations focused on the mechanisms and kinetics of cap formation and healing of defects. Growth from both pure metallic and carbide particles was studied using *ab initio* calculations by Börjesson et al. and Page et al., both concluding that the growth is possible from both metallic and carbide particles.[16,17] Nucleation of SWNTs on nickel nanoclusters was also studied by Amara and co-workers using a tight-binding Monte Carlo (MC) model, focusing on the effect of the chemical potential.[18−20] The accuracy of *ab initio* methods, however, comes at the price of the short time scales these methods can simulate in conjunction with the small system sizes they can handle. Therefore, dedicated interatomic potentials were developed to be used in classical MD simulations, in order to study CNT growth as well.

The first classical MD simulations were performed by Maiti et al.,[21,22] albeit without taking into account the metal atoms explicitly. Shibuta et al.[23] reported the first classical MD simulations taking into account all atoms (carbon and metal). Large, defect-rich tubes were formed from a random distribution of a large number of carbon atoms and a small number of Ni atoms, corresponding to a laser ablation process. Shibuta et al. also investigated the catalytic chemical vapor deposition (CVD) process by the impingement of C-atoms on small nickel clusters at 2500 K.[24] The effect of the substrate on the catalytic particles during SWNT growth was also studied.[25] A layered metal structure and a graphene layer parallel to the substrate were formed in the case of strong cluster−substrate interaction, while the metal did not adopt a specific orientation and the graphene sheet separated from the cluster in a random direction in the case of weak metal−substrate interaction.

Balbuena and co-workers updated the Shibuta potential and presented a step-by-step overview of the observed SWNT growth process.[26,27] Ribas et al.[28] and Burgos et al.[29] applied this potential to investigate the effect of the adhesion strength of the graphitic cap to the catalyst and of the temperature on the SWNT growth. The catalyst encapsulation was found to depend on the work of adhesion at $T > 600$ K. At lower temperature, limited carbon diffusion appeared to hinder the cap formation and cap lift-off.

Numerous simulations were performed by Ding et al. to investigate the influence of various parameters and growth conditions on the growth mechanism. The growth mechanism was found to shift from bulk diffusion mediated to surface diffusion mediated around 900−1000 K.[30] Larger clusters resulted in an enhanced growth of SWNTs compared to smaller clusters. Further, it was found by this group that while a temperature gradient may be important for larger particles, it is not required for SWNT growth from small particles.[31,32]

Unfortunately, however, all of these simulations suffer from two rather fundamental drawbacks: first, they lack long-range interactions as well as polarizable charges, and second, the time scale is still too short to take into account relaxation effects which would enable defects to be healed out.

To overcome the first problem, we employ the so-called Reactive Force Field (ReaxFF) interatomic potential, which is based on a bond distance−bond order relationship on the one hand, and a bond order−bond energy relationship on the other hand. ReaxFF also allows us to incorporate limited nonlocality (to mimic quantum behavior).[33] In contrast to previously used potentials, the ReaxFF potential also includes long-range van der Waals and Coulomb interactions and allows for polarization. Since ReaxFF is able to describe not only covalent bonds but also ionic bonds and the whole range of intermediate interactions, it has been successfully applied to nearly half of the periodic table of the elements and their compounds (see, e.g., refs 34−36 and references therein), typically showing dissociation and reactive potential curves in very good agreement with DFT results. In the present paper, we use the ReaxFF potential with parameters developed by Mueller et al.[34]

As a result of the second problem mentioned above, i.e., the neglect of relaxation effects, typical simulation results obtained with previous MD methods showed highly defected structures. To overcome this problem, we recently coupled our MD model to a force-biased Monte Carlo (fbMC) model to take into account these relaxation effects.[37−39]

It was demonstrated that by using the ReaxFF potential in conjunction with this hybrid MD/MC approach, for the first time

the growth of nearly defect-free SWNTs in the gas phase could be simulated, resulting in a SWNT with a (12,4) chirality.[39] In the present paper, we report the simulation of the growth of a SWNT on a surface-bound catalyst particle, which is more realistic, as it corresponds to the majority of the experimental growth studies. Moreover, as chirality is one of the most important properties of SWNTs, we will focus here especially on the evolution of the chirality during the growth. To our knowledge, this was not yet studied before. It will be demonstrated that various processes not observed earlier might be of importance during the growth of SWNTs, including the appearance and disappearance of nucleated caps and a changing cap chirality during the initial growth stage.

2. COMPUTATIONAL METHODOLOGY

2.1. Hybrid Molecular Dynamics/Monte Carlo. The procedure to simulate the growth of the SWNT is similar to our previously reported calculations.[39] In short, alternating MD and MC stages are used to simulate the addition of carbon to the cluster and relaxation processes, respectively. In the MD stage, a new carbon atom is added to the simulation box every 2 ps, provided there are no free carbon atoms in the simulation box. Hence, the number of free carbon atoms in the simulation box is at most one at all times. The free carbon atom then travels through the box until it impinges on the metal cluster. Every 4 ps, the resulting configuration is relaxed using the MC procedure. During this stage, no new carbon atoms are added to the system. After relaxation, the resulting configuration is again subjected to C-impacts in the next MD stage, etc. The equations of motion in the MD stage are solved using the velocity verlet scheme, using a time step of 0.25 fs. In the MC simulation stage, the structure is allowed to relax for 10^4 steps at a MC temperature of 1000 K. The maximum displacement of the carbon atoms in the MC algorithm is set to 0.12 Å in each Cartesian coordinate.

Note that the carbon addition rate results in a MD pressure that is in fact much too high to obtain SWNT growth. However, in the current simulation setup, this MD pressure does not correspond to the actual simulation growth pressure, since relaxation is taken into account by means of the MC stage, during which no carbon atoms are added.

Typically, SWNT growth simulations assume a gas-phase process. Experimentally, however, the majority of the growth results are obtained on surface-bound catalysts. Therefore, in the present paper, we consider a surface-bound Ni_{40} nanocluster as the catalyst, of which the lower eight atoms are kept static, similar to the simulations of Awano et al.[40] This fixed plane corresponds to a Ni(100) plane, in order to minimize possible epitaxy between the cluster and the growing carbon network induced by the presence of the fixed layer. Additionally, a virtual reflective boundary is applied, such that the C-atoms can only impinge on the cluster from above the surface. Note that this setup should be regarded as a model system, approximating the real substrate−nanocluster interaction only to first order. Indeed, certain important factors such as the wettability of the cluster on the surface or the cluster mobility on the surface cannot be captured in this approximation. We did not observe a change in the mobility of the mobile nickel atoms due to the presence of the fixed layer at this temperature (1000 K).

The initial structure of the nickel nanoparticle was a liquid droplet, generated by a heating−thermalization−relaxation procedure at 1000 K. During the growth, the cluster is thermostatically kept at a temperature of 1000 K using the Berendsen thermostat, using a coupling constant of 100 fs. The use of a sufficiently large ratio between the thermostat coupling constant and the MD time step ensures that the simulation is close to the microcanonical ensemble, while keeping the temperature on average constant. Since the thermostat only controls

the average temperature, we use separate temperature controls for C and Ni atoms, preventing divergence of their respective temperatures.

Although the size of the nanocluster is rather small, it is sufficient to identify all essential processes, and it significantly reduces the required computational time. Note that the complexity of ReaxFF and the coupling to the MC calculation limits the size of the system that can be handled in a reasonable time. The calculation of a single cap growth process currently takes typically several months on a single processor. New developments in parallel ReaxFF will facilitate future applications to larger systems.[41,42] Also, it should be realized that the simulation of a single trajectory bears no statistical significance. The current results therefore only demonstrate that certain processes which were previously not observed in any other simulated growth study may effectively occur and may be of importance for the growth of SWNTs.

2.2. Interatomic Interactions. All interatomic interactions are determined by the Reactive Force Field (ReaxFF).[33,34] ReaxFF is based on the bond order—bond distance relationship introduced by Abel[43] and applied to carbon by Tersoff[44] and to hydrocarbons by Brenner.[45]

The total system energy is written as a sum of several partial energy terms, related to the bond energy, lone pairs, under-coordination, over-coordination, valence and torsion angles, conjugation, and hydrogen-bonding as well as van der Waals and Coulomb interactions. Similar to our previous study, we employ a standard repulsive Lennard-Jones (LJ) potential to prevent the direct addition of gas-phase carbon atoms to the carbon network. This procedure mimics the instantaneous catalysis of hydrocarbons at the catalyst surface.[24,28]

3. RESULTS AND DISCUSSION

Before focusing on the growth mechanisms and chirality determination, we will first demonstrate the accuracy of the ReaxFF potential for structures and their energetics relevant to catalytic SWNT growth.

3.1. Validation of ReaxFF for Catalyzed SWNT Growth. Catalytic SWNT growth involves a number of atomic processes. These processes include diffusion of carbon in the bulk and at the surface of the nanocatalyst, segregation processes of carbon atoms at the surface, and the formation of graphene-like structures that can evolve in a SWNT cap. Simulating these processes requires the use of a transferable, highly accurate potential energy function that is able to describe the competition between the various carbon phases correctly. To validate the use of the current ReaxFF parametrization, we have therefore carried out various tests on fundamental properties of the Ni/C system.

A key parameter for the current study is the formation enthalpy of Ni—C compounds. The formation enthalpy is a measure of the competition between ordering and phase segregation tendencies.[18,20] In the case of Ni/C, the equilibrium phase diagram shows a tendency of phase separation, and hence the formation enthalpy must be positive. On the other hand, metastable Ni_3C can be produced, and hence the formation enthalpy cannot be too positive. Formation enthalpies were used to fit ReaxFF parameters for nickel at various densities in face-center cubic (fcc), body-center cubic (bcc), a15, simple cubic, and diamond crystal structures as determined from *ab initio* calculations.[34] For an accurate description of nickel-catalyzed (hydro)carbon chemistry, the ReaxFF parameters relevant to C—Ni bonding were optimized to fit an extensive set of binding energies for (hydro)carbons at nickel surface, subsurface, and bulk sites. Furthermore, because there are situations in which the catalyst particle is likely to form a nickel carbide, the same parameters were simultaneously optimized against formation enthalpies obtained from *ab initio* calculations for Ni_3C, Ni_2C,

and the B_1, B_2, B_3, and B_4 phases of NiC. A complete description of the results of the fitting procedure can be found in ref 34. These results demonstrate the ability of the current parametrization to reproduce all equations of state for the relevant structures, as well as its accuracy in predicting the reactive energy surfaces of hydrocarbons interacting with nickel.

A quantity related to the heat of formation is the heat of solution, which is experimentally found to be equal to 0.43 eV, whereas first-principles methods provide values of about 0.20—0.36 eV.[46] Using a tight-binding model, Amara et al.[47] obtained a value of 0.40 eV. We have calculated the heat of solution at 0 K for a C atom in bulk Ni as

$$\Delta H = E_p(Ni_xC) - (E_p(Ni_x) + E_p(C))$$

where $E_p(Ni_xC)$ is the minimized energy of the 3D periodic Ni_x crystal containing the dissolved C atom in an octahedral position ($x = \{32,108,832\}$), $E_p(Ni_x)$ is the minimized energy of the 3D periodic Ni_x crystal, and $E_p(C)$ is the potential energy of a single C atom at infinite distance from the Ni crystal, hence equal to 0. We have calculated the heat of solution to be 0.68, 0.73, and 0.76 eV for the Ni_{32}, Ni_{108}, and Ni_{832} structures, respectively, which is in fair agreement with both the experimental and theoretical results, albeit slightly too high. This result indicates that ReaxFF correctly predicts that the dissolution of carbon from graphite into bulk nickel (as a solid solution) is an endothermic process.

Further, the clustering energy of carbon atoms in the bulk of a nickel crystal is another quantifier of the tendency of carbon atoms to form carbon structures (e.g., dimers, trimers, rings, a carbon network, etc.). We have found a binding energy E_b of C atoms in nearest-neighbor octahedral sites of $E_b = 0.125$ eV (correctly predicting that the C—C interaction in the bulk of the Ni-crystal is repulsive), in good agreement with the *ab initio* data of Siegel et al., reporting values in the range $E_b = -0.010$ to 0.270 eV.[46]

To assess the accuracy of ReaxFF with respect to typical CNT defects, we have previously calculated the uncatalyzed energy barrier for the 5775 Stone—Wales defect.[39] A value of about 8.9 eV was obtained for the defect formation (upper boundary), which is close to the *ab initio* value of 8.6 eV reported by Zhao et al.[48] and the tight-binding value of 8.5 eV reported by Zhang et al.[49] The energy barrier for the uncatalyzed back reaction is calculated to be 6.0 eV (upper boundary), close to the tight-binding value[49] of 5.5 eV. This indicates that typical CNT defects are indeed metastable, unless they can be healed by a metal-mediated mechanism.[14]

Besides verifying relevant energetics of the Ni/C system, we have also verified critical configurational properties. Since the C—Ni bond length is in the order of 2.0 Å, while the available distance in fcc octahedral sites is only $a/2 = 1.76$ Å, the nickel crystal deforms upon incorporation of C in the lattice. This deformation is quantified by the formation volume V^F of a C interstitial and is defined as

$$V^F = V(Ni_x + C) - x\Omega_0(Ni)$$

where $V(Ni_x+C)$ is the volume of the relaxed Ni_xC structure and $\Omega_0(Ni)$ is the volume per atom of elemental Ni. For the octahedral site, we found $V^F = 0.66 \Omega_0$ for the $Ni_{832}C$ structure and $V^F = 0.71 \Omega_0$ for the $Ni_{32}C$ structure. These values are in close agreement with the *ab initio* data of Siegel et al., reporting values in the range $V^F = 0.64$—$0.80 \Omega_0$.[46]

These results indicate that the current ReaxFF potential is indeed sufficiently accurate to model the interaction between
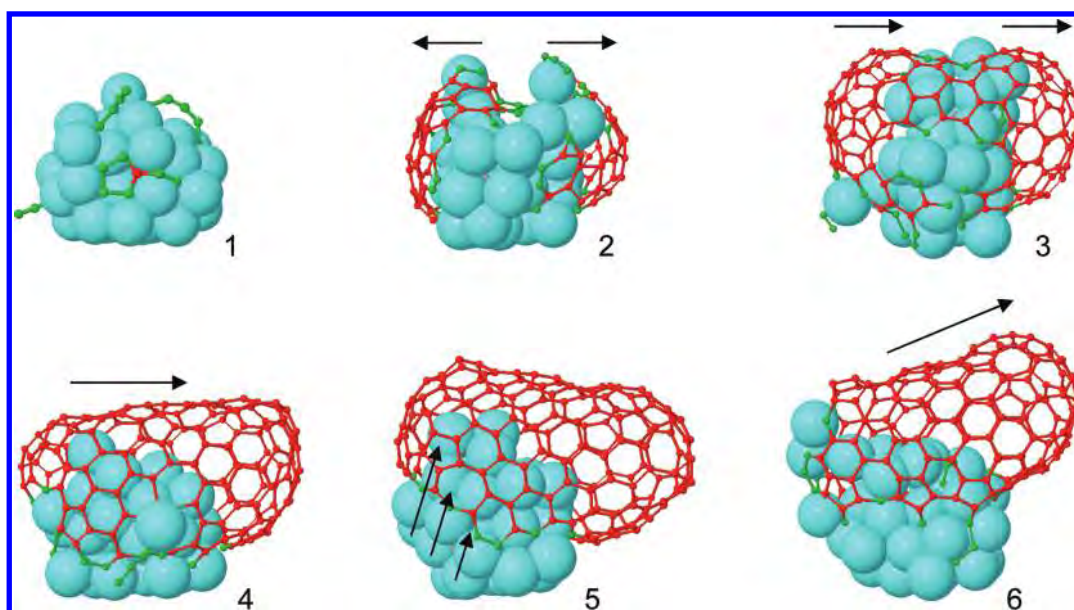
Figure 1. Simulated growth evolution. Arrows indicate the growth or elongation direction of the carbon network. (1) Carbon dissolution and first pentagon formation. (2) Two graphitic patches are formed. (3) These graphitic patches develop into two small caps. First "chirality" is visible (not metallic). (4) The carbon network slides over the cluster. In this process, one cap grows while the other cap disappears. Here, the chirality is changing. This step takes a very long time. (5) The carbon keeps on moving over the metal cluster until part of the metal is freed from the network (indicated by the arrows pointing upward), allowing new C-atoms to be incorporated. (6) At the end of the sliding process, the final chirality is obtained. (i.e., (7,7) metallic; see further).

carbon and carbon structures and a nickel substrate, regarding both the energetic aspects and the structural aspects. Furthermore, as most of these test cases were not included in the original ReaxFF force field development for Ni/C/H systems,[23] this good agreement indicates the transferability of the ReaxFF method to structures outside of its original training set.

3.2. SWNT Growth Process. The observed growth process is depicted in Figure 1 and can be described as follows. Initially, all impinging carbon atoms dissolve into the metal cluster. In this stage, our simulations predict that they preferentially occupy subsurface sites, in agreement with various tight-binding simulations.[12,19,47] When the carbon concentration in the bulk of the nanoparticle reaches a critical value of about 20%, carbon surface segregation starts to occur. In agreement with recent DFT/tight-binding calculations, the carbon ordering at the surface is predicted to change rapidly from initially isolated C-atoms to dimers and trimers, by metal-assisted carbon surface diffusion.[16] Subsequently, the first rings start to appear. Invariably, the first stable rings to be formed appear to be pentagons, again in agreement with previous DFT/tight-binding calculations.[11] The continued addition of carbon to the system leads to the formation of longer surface chains, corresponding to recent DFT/tight-binding simulations of SWNT growth on Ni.[13] These chains may rearrange, resulting in the formation of new rings. Concatenated ring systems, and ultimately graphitic islands, are thus formed. These islands seem to continue to grow into two SWNT caps in the present case. When a cap is sufficiently large, it remains attached to the metal nanoparticle only by its edge atoms. Addition of carbon atoms to these edges allows the growth of the SWNT from the cap(s). Although in the present paper we use a surface-bound catalyst particle on which the growth proceeds, the observed growth process appears to be very similar to the growth process we observed earlier in the case of
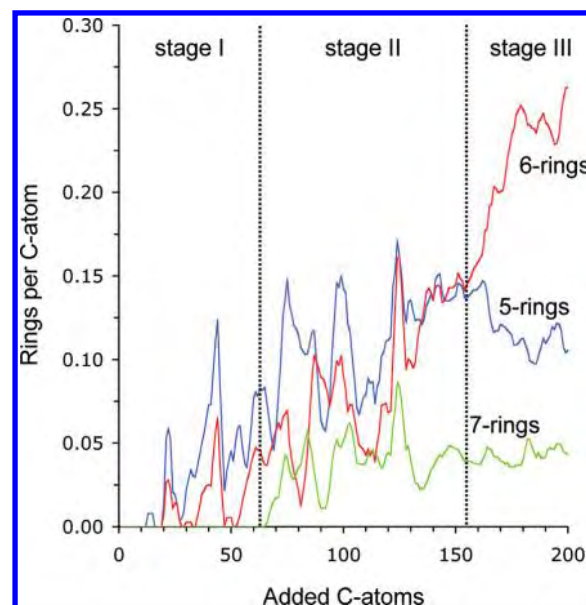

Figure 2. Evolution of the number of rings formed per added carbon atom. Three stages are observed. In stage I, 5-rings and 6-rings are formed; in stage II, rings start to concatenate, and also 7-rings are formed; in stage III, the metal-mediated healing of defects leads to a steep increase in the number of 6-rings, while the number of 5-rings and 7-rings stagnates.

gas-phase growth.[39] However, we also observe that while one of the caps slowly grows, the other cap disappears; in fact, a large number of highly concerted processes take place (including re-dissolution of carbon atoms in the cluster, addition of new carbon atoms to the structure, and formation of new C—C bonds), resulting in a net "sliding" of the carbon structure over the metal

cluster, thereby healing many topological defects (pentagon, heptagons, Stone—Wales defects, etc.), as will be described in more detail below. This process also induces a steep increase in the number of hexagons and a stagnation in the number of pentagons and heptagons (see below). This process was not observed earlier in our gas-phase simulations. Subsequently, when the carbon network has shifted entirely to one side of the metal cluster, the bottom part of the metal particle is freed from the network. Indeed, we observe that the carbon network is displaced away from the bottom of the cluster over a distance of a few angstroms. This process seems necessary to allow continued growth in the present simulation. Indeed, through this process, a new free metal surface is created, on which gas-phase carbon atoms can adsorb and continue the SWNT growth. This process was not observed in our previous gas-phase growth simulations.[39]

In Figure 2, the evolution of the number of polygons formed in the nucleation process is plotted as a function of the number of carbon atoms added to the system. Three stages can be discerned: a first stage in which only 5- and 6-rings are formed, a second stage in which also 7-rings are created, and a third stage in which the number of 6-rings steeply increases whereas the number of 5- and 7-rings per incorporated C-atom stagnates. It is clear from the figure that pentagons and hexagons are the primary components of the carbon network in the initial nucleation stage, corresponding to observations in DFT/tight-binding simulations.[11] Indeed, in this initial stage (up to about 70 carbon atoms added), only 5- and 6-rings are formed, with a slight preference for pentagon formation. This preference is related to their higher stability on the convex surface of the metal cluster.[50] In this stage, we observed that the rings do not yet form a network. Rather, the surface is covered by lone rings and polyyne chains.

The second stage is initiated by the increasing carbon coverage on the surface. Indeed, when a critical carbon concentration is reached at the surface, the addition of more carbons, on the one hand, and the continuous rearrangement of existing carbon polyyne surface chains, on the other hand, lead to the formation of concatenated rings—the first cap nuclei, in agreement with tight-binding MC calculations.[20] The initiation of this stage is indicated by the occurrence of the first heptagons. This process continues as outlined above, allowing the ring networks to grow.

The third stage starts as soon as the two caps are formed (see Figure 1). The steep increase in the number of hexagons and the stagnation in the number of pentagons and heptagons are due to the metal-mediated healing, as explained below. In absolute numbers, the number of hexagons increases in this stage from 23 to 52, while the number of pentagons remains essentially constant, and the number of heptagons increases only marginally, from 6 to 8.

During the initial nucleation stage, a few metal atoms are observed to detach (temporarily) from the cluster. Indeed, the metal atoms are observed to be rather mobile in this stage, leading to a partial disintegration of the metal cluster. This is a result of the nickel electron depletion due to the polarization of the system; i.e., the more electronegative carbon atoms attract some charge from the nickel atoms, which become slightly positive (electron depleted), causing the partial disintegration. As the first concatenated carbon systems are formed on the surface of the particle, however, these carbon atoms keep the metal cluster together and reduce the charge polarization by
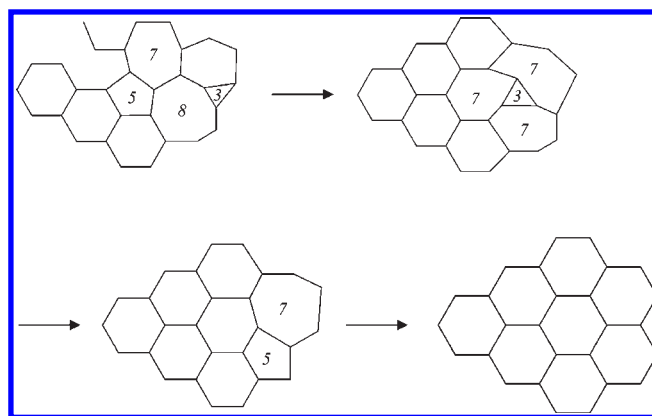

Figure 3. Illustration of defect healing observed in the simulations during the sliding process.

reducing the area of metal—carbon interface, as was also observed by Ohta et al.[11]

Defect Healing. It has been argued that the insertion of carbon atoms into the reactive metal—carbon boundary is an intrinsically random process, thus (randomly) forming pentagons, hexagons, and heptagons at the base of the SWNT structure.[14] Consequently, SWNT growth itself is also intrinsically random, thus leading to a structure lacking a clear (n,m) chirality.[12] However, it has also been observed, by us and other groups, that the metal assists in healing these topological defects.[14,15,39,47]

In the current simulation, we observe that many defects are healed by the restructuring process in which the carbon network slides over the metal particle. While metal-mediated defect healing was also observed in our earlier gas-phase simulations, the sliding process was previously not observed. An example of a defect healing process observed in our simulations is illustrated in Figure 3. It is clear that the network initially contains a number of defects, including a triangle, a pentagon, a heptagon, and an octagon. These defects are healed in a stepwise fashion. First, the defected network is rearranged into three heptagons surrounding the triangle. This defect is then healed into a 5—7 defect, which subsequently heals into a perfect network of all hexagons. This healing process does not occur fast but rather over a large number of consecutive MD/MC cycles. This explains why such healing processes were not observed earlier in pure MD simulations. Also, these processes should be understood as concerted reactions and not as individual consecutive isolated events.

The restructuring process also has a profound effect on the ring formation. Indeed, the healing of defects transforms pentagons and heptagons into hexagons, leading to a steep increase in the number of hexagons (as was illustrated in Figure 2). The addition of new carbon atoms to the carbon network also forms new rings, including pentagons and heptagons. Therefore, overall, the number of pentagons and heptagon remains essentially constant, while the number of hexagons increases.

Evolution of Chirality. The restructuring and associated defect healing processes have a profound influence of the resulting chirality evolution, as shown in Figure 4. In this figure, the axial direction of the carbon network is drawn vertical for all structures. Early in the nucleation stage, a first band of concatenated hexagons can be seen, forming a SWNT cap with a diameter $D = 8.5$ Å and a chiral angle $\theta = 0°$. The (n,m) indices can then be obtained from the lattice parameter a of graphene, the diameter,
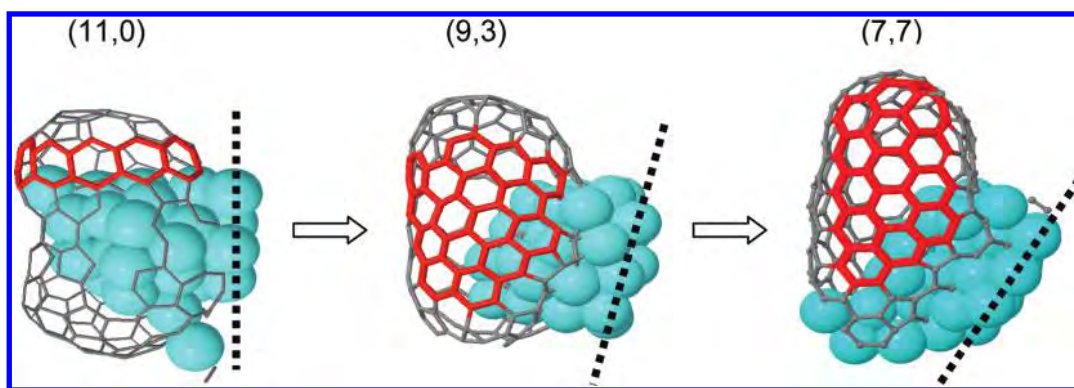
Figure 4. Evolution of chirality during the growth process. The chirality of the different structures, as defined by its diameter and chiral angle, is indicated above each structure. The dotted line indicates the surface.

and the chiral angle,

$$\theta = \tan^{-1}\left(\frac{\sqrt{3}m}{2n + m}\right)$$

$$D = \frac{a}{\pi}\sqrt{n^2 + nm + m^2}$$

corresponding to a zigzag configuration with (11,0) chirality. This chirality, however, is only transitory, and the cap should be regarded as a nascent higher-angle cap. Note that, related to this, it was previously demonstrated that in the early nucleation stage, (near-)armchair caps have edges that appear to be dominated by zigzag edges.[9] Further, it should be noticed that no chirality could be assigned to the second cap (i.e., the cap that subsequently disappears), due to the presence of too many defects. It is clear that the (11,0) chirality is not preserved in the subsequent elongation of the cap, as is obvious from Figure 4. Indeed, the chiral angle is observed to change, while the diameter of the cap remains about 8.5 Å. For the second structure in Figure 4, the chiral angle was determined to be $\theta = 14°$, corresponding to a chiral structure with a (9,3) chirality. This change in chiral angle is induced by the restructuring process: indeed, a change in chirality is induced when a defect (such as a 5—7 defect) is not healed by the restructuring process but is incorporated in the tube. Note, however, that the introduction of, e.g., a pair of 5—7 defects (i.e., a Stone—Wales defect) does not introduce this chirality change.[51—53] The dotted lines in the figure indicate the position of the surface. Hence, it is also clear from the figure that the SWNT does not maintain its orientation relative to the substrate but rather constantly changes during the process. After the restructuring process is completed, a metallic armchair SWNT emerges with a (7,7) chirality, as can be deduced from Figure 4. While the (7,7) chirality observed at the end of our simulation is not necessarily the final chirality, the rate of carbon addition to the cluster at this point in the simulation became so slow that further growth was not attempted because of the prohibitively long calculation times. Thus, our simulations predict that the chirality is not necessarily determined during the initial cap formation stage or cap lift-off and then remains fixed, but rather it can still change during the restructuring process in which many—but not all—topological defects in the carbon network are healed by the action of the metal catalyst. Note that the observed chirality change is from low-chiral-angle to high-chiral-angle. This observation is in agreement with DFT

calculations, showing that the growth of (near-)armchair structures is both kinetically and thermodynamically favored.[9]

Finally, also note that, in this process of changing chirality, also the rim of the tube is continuously changing: it is composed of zigzag, armchair, and Klein edges, formed not only by hexagons but also by pentagons and heptagons. This continuous transformation of the edge is induced by the continuous addition of new carbon atoms and the metal-induced carbon network restructuring process.

4. SUMMARY AND CONCLUSIONS

Hybrid molecular dynamics/force-biased Monte Carlo simulations were used to simulate the growth of SWNT on a substrate-bound Ni_{40} cluster. The force field used is the Reactive Force Field (ReaxFF), and relaxation effects are taken into account by coupling the MD simulation to MC simulations. In the growth process, two caps are initially formed, of which one continues to grow while the other disappears again. It is observed that the carbon network is restructured through a metal-mediated process. During this process, many topological defects are healed, and the chirality is observed to change, from (11,0) to (9,3). After the restructuring process is completed, a metallic SWNT with a (7,7) armchair chirality emerges. Finally, it is also observed that encapsulation of the nanocatalyst is prevented by a migration of the entire carbon network over the metal surface. These calculations demonstrate for the first time the simulated growth of an armchair SWNT with a definite chirality on a surface-bound catalyst.

■ AUTHOR INFORMATION

Corresponding Author
erik.neyts@ua.ac.be

■ ACKNOWLEDGMENT

the Flemish Government (department EWI), and the Universiteit Antwerpen.

■ REFERENCES

(1) Saito, R.; Dresselhaus, G.; Dresselhaus, M. S. In *Physical properties of carbon nanotubes*; Imperial College Press: London, 1998.

(2) Boughmann, R. H.; Zakhidov, A. A.; de Heer, W. A. *Science* **2002**, *297*, 787–792.

(3) Sazonova, V.; Yaish, Y.; Üstünel, H.; Roundy, D.; Arias, T.; McEuen, P. L. *Nature* **2004**, *431*, 284–287.

(4) Song, W.; Jeon, C.; Kim, Y. S.; Kwon, Y. T.; Jung, D. S.; Jang, S. W.; Choi, W. C.; Park, J. S.; Saito, R.; Park, C.-Y. *ACS Nano* **2010**, *4*, 1012–1018.

(5) Chiang, W.-H.; Sankaran, R. M. *Nat. Mater.* **2010**, *8*, 882–886.

(6) Chiang, W.-H.; Sakr, M.; Gao, X. P. A.; Sankaran, R. M. *ACS Nano* **2009**, *3*, 4023–4032.

(7) Gavillet, J.; Loiseau, A.; Journet, C.; Willaime, F.; Ducastelle, F.; Charlier, J.-C. *Phys. Rev. Lett.* **2001**, *87*, 275504.

(8) Gavillet, J.; Loiseau, A.; Ducastelle, F.; Thair, S.; Bernier, P.; Stéphan, O.; Thibault, J.; Charlier, J.-C. *Carbon* **2002**, *40*, 1649–1663.

(9) Gómez-Gualdrón, D. A.; Balbuena, P. B. *Nanotechnology* **2008**, *19*, 485604.

(10) Wang, Q.; Ng, M.-F.; Yang, S.-W.; Yang, Y.; Chen, Y. *ACS Nano* **2010**, *2*, 939–946.

(11) Ohta, Y.; Okamoto, Y.; Page, A. J.; Irle, S.; Morokuma, K. *ACS Nano* **2009**, *3*, 3413–3420.

(12) Ohta, Y.; Okamoto, Y.; Irle, S.; Morokuma, K. *ACS Nano* **2008**, *2*, 1437–1444.

(13) Page, A. J.; Minami, S.; Ohta, Y.; Irle, S.; Morokuma, K. *Carbon* **2010**, *48*, 3014–3026.

(14) Page, A. J.; Ohta, Y.; Okamoto, Y.; Irle, S.; Morokuma, K. *J. Phys. Chem. C* **2009**, *113*, 20198–20207.

(15) Page, A. J.; Ohta, Y.; Irle, S.; Morokuma, K. *Acc. Chem. Res.* **2010**, *43*, 1375–1385.

(16) Page, A. J.; Yamane, H.; Ohta, Y.; Irle, S.; Morokuma, K. *J. Am. Chem. Soc.* **2010**, *132*, 15699–15707.

(17) Börjesson, A.; Bolton, K. *J. Phys. Chem. C* **2010**, *114*, 18045–18050.

(18) Amara, H.; Roussel, J.-M.; Bichara, C.; Gaspard, J.-P.; Ducastelle, F. *Phys. Rev. B* **2009**, *79*, 014109.

(19) Moors, M.; Amara, H.; de Bocarmé, T. V.; Bichara, C.; Ducastelle, F.; Kruse, N.; Charlier, J.-C. *ACS Nano* **2009**, *3*, 511–516.

(20) Amara, H.; Bichara, C.; Ducastelle, F. *Phys. Rev. Lett.* **2008**, *100*, 056105.

(21) Maiti, A.; Brabec, C. J.; Roland, C.; Bernholc, J. *Phys. Rev. B* **1995**, *52*, 14850–14858.

(22) Maiti, A.; Brabec, C. J.; Bernholc, J. *Phys. Rev. B* **1997**, *55*, R6097–100.

(23) Shibuta, Y.; Maruyama, S. *Physica B* **2002**, *323*, 187–189.

(24) Shibuta, Y.; Maruyama, S. *Chem. Phys. Lett.* **2003**, *382*, 381–386.

(25) Shibuta, Y.; Maruyama, S. *Chem. Phys. Lett.* **2007**, *437*, 218–223.

(26) Martinez-Limia, A.; Zhao, J.; Balbuena, P. B. *J. Mol. Modell.* **2007**, *13*, 595–600.

(27) Zhao, J.; Martinez-Limia, A.; Balbuena, P. B. *Nanotechnology* **2005**, *16*, S575–581.

(28) Ribas, M. A.; Ding, F.; Balbuena, P. B.; Yakobson, B. I. *J. Chem. Phys.* **2009**, *131*, 224501.

(29) Burgos, J. C.; Reyna, H.; Yakobson, B. I.; Balbuena, P. B. *J. Phys. Chem. C* **2010**, *114*, 6952–6958.

(30) Ding, F.; Rosén, A.; Bolton, K. *Carbon* **2005**, *43*, 2215–2217.

(31) Ding, F.; Bolton, K.; Rosén, A. *Comput. Mater. Sci.* **2006**, *35*, 243–246.

(32) Ding, F.; Rosén, A.; Bolton, K. *Chem. Phys. Lett.* **2004**, *393*, 309–313.

(33) van Duin, A. C. T.; Dasgupta, S.; Lorant, F.; Goddard, W. A., III *J. Phys. Chem. A* **2001**, *105*, 9396–9409.

(34) Mueller, J. E.; van Duin, A. C. T.; Goddard, W. A., III *J. Phys. Chem. C* **2010**, *114*, 5675.

(35) Buehler, M. J.; Tang, H.; van Duin, A. C. T.; Goddard, W. A., III *Phys. Rev. Lett.* **2007**, *99*, 165502.

(36) Garcia, A. P.; Buehler, M. J. *Comput. Mater. Sci.* **2010**, *48*, 303–309.

(37) Timonova, M.; Groenewegen, J.; Thijsse, B. J. *Phys. Rev. B* **2010**, *81*, 144107.

(38) Neyts, E. C.; Bogaerts *J. Phys. Chem. C* **2009**, *113*, 2771–2776.

(39) Neyts, E. C.; Shibuta, Y.; van Duin, A. C. T.; Bogaerts, A. *ACS Nano* **2010**, *4*, 6665–6672.

(40) Awano, Y.; Sato, S.; Kondo, D.; Ohfuti, M.; Kawabata, A.; Nihei, M.; Yokoyama, N. *Phys. Stat. Sol. a* **2006**, *203*, 3611–3616.

(41) Nakano, A.; Kalia, R. K.; Nomura, K.; Sharma, A.; Vashishta, P.; Shimojo, F.; van Duin, A. C. T.; Goddard, W. A.; Biswas, R.; Srivastava, D. *Comput. Mater. Sci.* **2007**, *38*, 642–652.

(42) Zybin, S. V.; Goddard, W. A., III; Xu, P.; van Duin, A. C. T.; Thompson, A. P. *Appl. Phys. Lett.* **2010**, *96*, 081918.

(43) Abell, G. C. *Phys. Rev. B* **1985**, *31*, 6184–6196.

(44) Tersoff, J. *Phys. Rev. Lett.* **1988**, *61*, 2879–2882.

(45) Brenner, D. W. *Phys. Rev. B* **1990**, *42*, 9458–9471.

(46) Siegel, D. J.; Hamilton, J. C. *Phys. Rev. B* **2003**, *68*, 094105.

(47) Amara, H.; Bichara, C.; Ducastelle, F. *Phys. Rev. B* **2006**, *73*, 113404.

(48) Zhao, Q.; Nardelli, M. B.; Bernholc, J. *Phys. Rev. B* **2002**, *65*, 144105.

(49) Zhang, P.; Lammert, P. E.; Crespi, V. H. *Phys. Rev. Lett.* **1998**, *81*, 5346–5349.

(50) Fan, X.; Buczko, R.; Puretzky, A. A.; Geohegan, D. B.; Howe, J. Y.; Pantelides, S. T.; Pennycook, S. J. *Phys. Rev. Lett.* **2003**, *90*, 145501.

(51) Deguchi, H.; Yamaguchi, Y.; Hirahara, K.; Nakayama, Y. *Chem. Phys. Lett.* **2011**, *503*, 272–276.

(52) Saito, R.; Yakobson, B. I.; *Proceedings of the symposium on Recent Advances in the Chemistry and Physics of Fullerenes and Related Materials*, volume 5; Kadish, K. M., Ruoff, R. S. (Eds.), The Electrochemical Society, Pennington, New Jersey, United States, 1997.

(53) Yakobson, B. I. *Appl. Phys. Lett.* **1998**, *72*, 918–920.